Near-quantum-limited haloscope search for dark-photon dark matter enhanced by a high-Q superconducting cavity

Runqi Kang,[1,2,3] Man Jiao,[1,4] Yu Tong,[1,2] Yang Liu,[5] Youpeng Zhong,[6,5] Yi-Fu Cai,[7,8] Jingwei Zhou,[1,2,3,*] Xing Rong,[1,2,3,†] and Jiangfeng Du[1,2,3,4,‡]

[1]*CAS Key Laboratory of Microscale Magnetic Resonance and School of Physical Sciences, University of Science and Technology of China, Hefei 230026, China*
[2]*CAS Center for Excellence in Quantum Information and Quantum Physics, University of Science and Technology of China, Hefei 230026, China*
[3]*Hefei National Laboratory, Hefei 230088, China*
[4]*Institute of Quantum Sensing and School of Physics, Zhejiang University, Hangzhou 310027, China*
[5]*International Quantum Academy, Shenzhen 518048, China*
[6]*Shenzhen Institute for Quantum Science and Engineering, Southern University of Science and Technology, Shenzhen, China*
[7]*Deep Space Exploration Laboratory/School of Physical Sciences, University of Science and Technology of China, Hefei, Anhui 230026, China*
[8]*CAS Key Laboratory for Researches in Galaxies and Cosmology/Department of Astronomy, School of Astronomy and Space Science, University of Science and Technology of China, Hefei, Anhui 230026, China*

(Received 20 September 2023; accepted 18 April 2024; published 24 May 2024)

We report new experimental results on the search for dark photons based on a near-quantum-limited haloscope equipped with a superconducting cavity. The loaded quality factor of the superconducting cavity is 6×10^5, so that the expected signal from dark-photon dark matter can be enhanced by more than one order compared to a copper cavity. A Josephson parametric amplifier with a near-quantum-limited noise temperature has been utilized to minimize the noise during the search. Furthermore, a digital acquisition card based on field programmable gate arrays has been utilized to maximize data collection efficiency with a duty cycle being 100%. This work has established the most stringent constraints on dark photons at around 26.965 μeV. In the future, our apparatus can be extended to search for other dark matter candidates, such as axions and axionlike particles, and scrutinize new physics beyond the Standard Model.

DOI: 10.1103/PhysRevD.109.095037

Dark matter is one of the most enigmatic and salient topics in modern physics [1–5]. Although there are abundant phenomena that point to dark matter, its existence yet remains a mystery [6–9]. The dark photon is an important candidate for dark matter and also a possible portal that connects the Standard Model sector and the dark sector. It is claimed to be helpful to explain many unsolved problems in physics, such as the velocity discrepancy of galaxies [6], cosmic ray anomaly [10,11], muon anomalous magnetic moment [12,13], and W-boson mass anomaly [14–16].

*zhoujw@ustc.edu.cn
†xrong@ustc.edu.cn
‡djf@ustc.edu.cn

The dark photon is a spin-1 massive boson that rises from a slight extension of the Standard Model [17–19]. It couples to the ordinary photon via the following Lagrangian:

$$\mathcal{L} = -\frac{1}{4}F_{\mu\nu}^2 - \frac{1}{4}V_{\mu\nu}^2 - \frac{m_{A'}^2}{2}A'_\mu A'^\mu + \frac{\chi}{2}F_{\mu\nu}V^{\mu\nu}, \quad (1)$$

where A_μ and A'_μ are the gauge fields of the ordinary photon and the dark photon, respectively, $F_{\mu\nu} = \partial_\mu A_\nu - \partial_\nu A_\mu$ and $V_{\mu\nu} = \partial_\mu A'_\nu - \partial_\nu A'_\mu$ are the corresponding electromagnetic field tensors, $m_{A'}$ is the mass of the dark photon, and χ is the kinetic mixing, through which the dark photon interacts with the ordinary photon. The dark-photon mass $m_{A'}$ is a free parameter that can take a wide range of values, while the kinetic mixing χ can be very small. These two features render the search for the dark photon an extremely challenging task.

The haloscope is one of the most widely used methods for dark-photon searching. It is based on the fact that dark

photons can convert to ordinary photons in a microwave cavity due to the kinetic mixing term [20–22]. The power of the dark-photon signal is

$$P_s(f) = \frac{m_{A'}\rho_{A'}}{\hbar}\chi^2 VC\frac{Q_L Q_a}{Q_L + Q_a}\frac{\beta}{1+\beta}L(f, f_c, Q_L), \quad (2)$$

where $\rho_{A'} = 0.45\ \mathrm{GeV/cm^3}$ is the density of dark matter [23], and β is the coupling coefficient between the cavity and the output port; f_c, V, C are the resonant frequency, volume, and filling factor of the cavity, respectively. Q_L and Q_a are the quality factor of the cavity and dark photons, respectively, and $L(f,f_c,Q_L)=[1+4(Q_L(f-f_c)/f_c)^2]^{-1}$ is the Lorentzian line shape. Many groups across the world have been working on searching for dark photons. Projects such as ORGAN [24], QUAX [25,26], and ADMX [27] use cavities to conduct resonant detections. The SQuAD experiment [28] utilizes qubits to enhance the sensitivity. Experiments like FUNK [29], BREAD [30], DOSUE [31], QUALIPHIDE [32], BRASS-p [33], and Dark SRF [34] utilize the nonresonant methods to achieve large bandwidths. The signal-to-noise ratio (SNR) of a haloscope system is typically limited by factors such as the quality factor and volume of the cavity, noise temperature, and data acquisition (DAQ) efficiency. Plentiful efforts have been made to improve the SNR of the detection systems. For example, HAYSTAC employed Josephson parametric amplifier (JPAs) to minimize the noise [35], while QUAX used a superconductive cavity with a high quality factor to increase the potential dark matter signal [36]. Groups like ADMX and CAPP fabricated cavities with large volumes to enhance the potential signal [27,37]. In order to further improve the searching ability, it is desirable to simultaneously push these key parameters to their limits. However, this is practically challenging due to factors such as frequency drifts, difficulties in fabrication of the high-Q, large-volume cavity, dead time of electronic devices, and compatibility issues.

Here we focus on a promising region of the dark-photon mass, which is on the order of tens of μeV [38–40]. In order to improve the SNR, a superconducting cavity with a high quality factor and a large volume was utilized to maximize the potential dark-photon signal. To minimize the noise, a JPA with a near-quantum-limited noise temperature was installed. Additionally, we employed a homemade DAQ card based on the field programmable gate array (FPGA) to achieve a 100% duty cycle [41]. The hitherto highest sensitivity to χ is achieved in a 0.4 neV region around 26.96514 μeV. While the constraints on χ have never touched the 10^{-16} line in prior searching efforts, this work sets an upper limit of χ of 6.0×10^{-16} at 90% confidence level at the center of the region.

Figure 1 shows the simplified diagram of the experimental setup (see more details in Sec. I of Supplemental Material [42]), which consisted of two main parts: the detection part for searching dark photons and the calibration part for calibrating significant parameters of the detection part. A temperature as low as 21 mK and extremely stable was achieved with a dilution refrigerator.

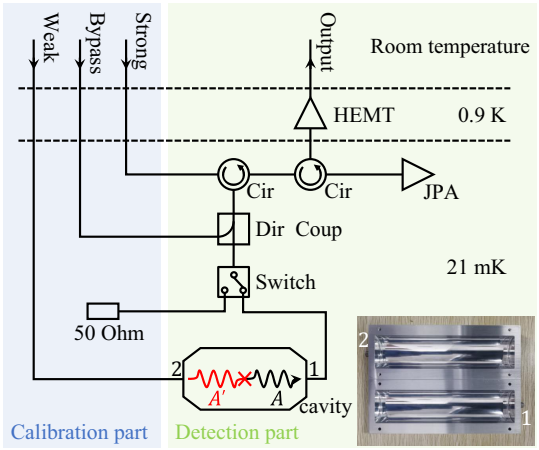

FIG. 1. Simplified diagram of the experimental apparatus. The green box stands for the detection part. It includes a cylindrical superconducting cavity of a high quality factor and an output line with an amplifier chain for the measurement of the signal. A' and A refer to the dark photon and the photon, respectively. The blue box stands for the calibration part. It includes three input lines and a 50 Ω load. The inset is a photograph of the cavity. Its inner side is finely polished for a high-Q factor. MW signals are coupled to the transmission lines through two coaxial probes. The two probes are fabricated on the opposite sides of the cavity to avoid their direct coupling.

The detection part is presented in the green box in Fig. 1. It includes a superconducting cavity, an amplification chain, and a DAQ card. The cylindrical superconducting cavity working at the TM_{010} mode performed as an antenna to collect the dark-photon signal. Dark photons inside the cavity would continuously oscillate into ordinary photons due to the kinetic mixing and then generate a microwave (MW) signal. The inset of Fig. 1 presents the picture of the superconducting cavity. The cavity was made of 6061 aluminum alloy, whose critical temperature is around 1 K. The inner side of the cavity was finely polished to enhance the Q factor. The diameter and length are 35.31 and 150.00 mm, respectively. The electric field of the TM_{010} mode is along the cylindrical axis of the cavity, thus the filling factor can be expressed as

$$C = \frac{|\int dV\mathbf{E}|^2}{V\int dV|\mathbf{E}|^2}\langle\cos^2\theta\rangle, \quad (3)$$

where θ stands for the angle between the polarization direction of the dark-photon field and the electric field. In the random polarization scenario, $\langle\cos\theta\rangle$ equals 1/3 [22,43]. The simulation result shows that the filling factor C is 0.23. There were two ports in the cavity: the strong one (port 1) for readout and the weak one (port 2) for injection

of a simulated dark-photon signal. The coupling from the cavity to the transmission lines was achieved through coaxial probes. In order to avoid direct coupling between the two probes, they were fabricated on the opposite sides of the cavity. The amplification chain was connected to port 1. A JPA accompanied by a circulator was taken as the first-stage amplifier since its noise temperature approaches the quantum limit $T_n = \hbar\omega/k_B$ [44]. The signal was further amplified by high-electron-mobility transistor (HEMT) amplifiers to a level where the electrical noise does not dominate and read out by a homemade DAQ card based on FPGAs (see more details in Sec. II of Supplemental Material [42]). The parallel sampling module and fast-Fourier-transform modules of the DAQ card allowed for simultaneous data collection and frequency spectrum calculation with a 100% duty cycle.

The calibration part is indicated by the blue box in Fig. 1. It aimed to measure significant parameters of the detection part, including the resonant frequency of the cavity and the noise temperature of the HEMTs. The strong line allowed for the measurement of the resonant frequency of the cavity. The 50 Ω load and a heater (not shown) played the role of a temperature-variable black radiation source, and a low-temperature switch supported convenient shift between the cavity and the 50 Ω load. They were used to measure the noise temperature of the HEMTs through the Y-factor method. The bypass line was used to measure the temperature noise and the gain of the JPA. The weak line was used for injection of a simulated dark-photon signal verification of the detection system (see more details in Sec. III of Supplemental Material [42]).

To locate the resonant frequency f_c of the cavity, the reflection coefficient of port 1 of the cavity was measured, as presented in Fig. 2(a). The result is fitted to the equation [45]

$$S_{11} = \alpha e^{i\psi}\left[1 - \frac{2\beta_1/(1+\beta_1)e^{i\phi}}{1 + 2iQ_L(f/f_c - 1)}\right], \tag{4}$$

where α and ψ are the power loss and the phase shift during transmission, respectively, and the parameter ϕ describes the impedance mismatch, which makes the spectrum asymmetric. The fitting gives $f_c = 6.52014$ GHz.

During the calibration of the HEMTs, the pumping of the JPA was off, and the switch was thrown to the 50 Ω load. The thermal noise power of the system can be expressed as

$$P_t = G_H B\left[hf_c\left(\frac{1}{e^{hf_c/k_B T_b} - 1} + \frac{1}{2}\right) + k_B T'_n\right], \tag{5}$$

where G_H is the gain of the HEMT chain, k_B is the Boltzmann constant, B is the bin width of the spectrum, T'_n is the noise temperature of the HEMT chain, and T_b is the physical temperature of the 50 Ω load. By varying T_b and fitting the temperature dependence of P_t, as plotted in Fig. 2(b), $G_H = 76.9 \pm 0.3$ dB and $T'_n = 1.9 \pm 0.1$ K are obtained.

The transmission coefficients from the bypass line to the output line as the pumping of the JPA was on and off are shown as the red and yellow lines in Fig. 2(c), respectively. The blue line refers to their difference, i.e., the gain of the JPA, which is 20 dB at the resonant frequency of the cavity. The noise temperature of the JPA T_n is calculated to be 297 ± 22 mK from the formula

$$T_n = \frac{1}{G_J}\frac{P_{J\_on}}{P_{J\_off}}T'_n, \tag{6}$$

where G_J is the gain of the JPA, and P_{J_on} and P_{J_off} are the thermal noise power measured from the output line with the JPA on and off, respectively. Since the bandwidth of the JPA is much broader than that of the cavity, its gain and noise temperature can be considered uniform in the detection region.

During the detection of dark photons, all the inputs except the pumping of the JPA were off. The data collection lasted for 6 h. Forty thousand raw spectra have been obtained. The frequency bin width B of each spectrum was 0.48 kHz. These raw spectra were divided into 100 subruns, each containing 400 raw spectra. The average of the first subrun is shown as the blue dots in Fig. 3(a). The line shape is right the resonant dip of the cavity.

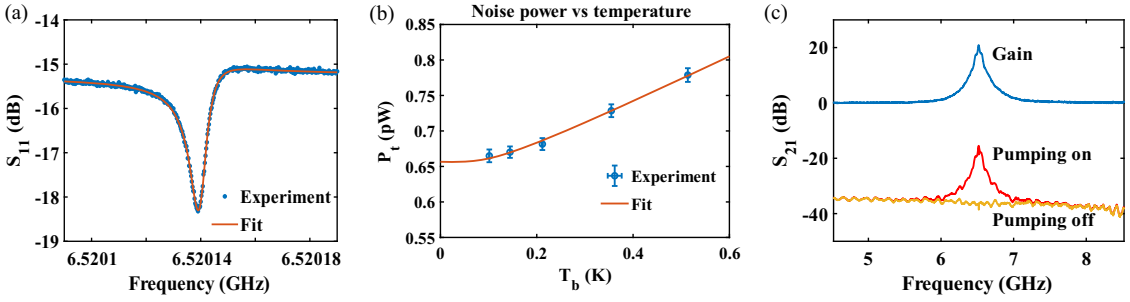

FIG. 2. Calibration results. (a) Reflection coefficients of port 1 of the cavity. The resonant frequency of the cavity f_c is 6.52014 GHz. (b) The relation between the noise power and the temperature of the 50 Ω load. The noise temperature of the HEMT chain T'_n is 1.9 K. (c) Calibration result of the gain of the JPA. The red and yellow lines refer to the transmission coefficients S_{21} from the bypass line to the output line when the JPA is on and off, respectively. Their difference is plotted as the blue line. The gain of the JPA at f_c is $G_J = 20$ dB.

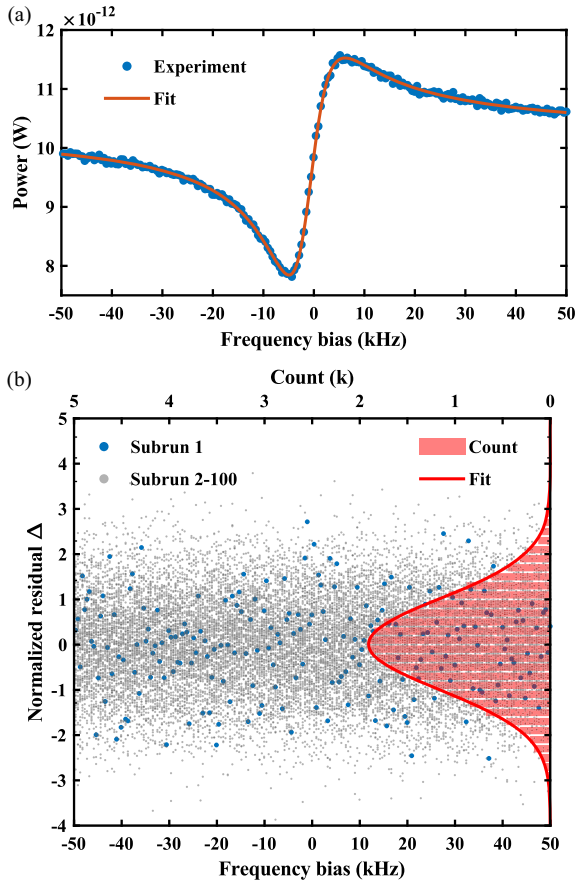

FIG. 3. (a) The power spectrum of the first subrun. The blue dots are the measured powers averaged from 400 raw spectra. Two consecutive fittings were used to remove the baseline due to the cavity and the MW devices. The product of the fitting results is shown as the orange line. (b) The normalized residuals Δ and their distribution. The normalized residuals obtained from subrun 1 and subruns 2–100 are plotted as the blue and gray dots, respectively. The red bars are the counts of data, while the red line is the fitting result, which is pretty close to the unit Gaussian distribution.

The spectra are first fitted to Eq. (4) (Fit_1) to remove the baseline due to the cavity. Then, the fluctuations in the transmission efficiency of the devices are removed by applying a sum-of-sines fitting (Fit_2). Meanwhile, the values of the coupling coefficient β_1 and the quality factor of the cavity Q_L during each subrun are obtained from the fitting results. The product of the two fitting results of the first subrun is shown as the orange line in Fig. 3(a), with $\beta_1 = 0.4$ and $Q_L = 6.1 \times 10^5$. The blue dots in Fig. 3(b) depict the standardized power residuals Δ of subrun 1,

$$\Delta = \frac{\Delta_s}{\sigma_s}, \tag{7}$$

where Δ_s is the normalized power excess obtained from the baseline removing operation, and σ_s is the standard deviation of the normalized power excess (see more details in Sec. IV of Supplemental Material [42]). The gray dots depict the standardized residuals of subruns 2–100.

A power excess over 5 times the standard deviation is required for a data point to be claimed as a candidate signal. To check the presence of any candidate signal in our results, the standardized power residuals are counted, as illustrated by the red bars in Fig. 3(b). The red line is the fitting result with the Gaussian distribution $\mathrm{N}(\mu, \sigma'^2)$, where μ is the mean value of the data and σ' is the standard deviation. The distribution of the standardized power residuals fits well with the unit Gaussian distribution, with $\mu = 0.009 \pm 0.010$ and $\sigma' = 1.009 \pm 0.010$. No power excess over 5σ is observed. Therefore, our results provide an exclusion of dark photons in the detection bandwidth.

The data analysis that provides the constraints of the kinetic mixing χ follows the method developed in the ADMX experiment [46] (see more details in Secs. IV and V of Supplemental Material [42]). Figure 4 shows the upper bounds on the kinetic mixing in the range of dark-photon masses from 26.96493 to 26.96534 μeV with a confidence level of 90%. The red line refers to the upper bounds of the kinetic mixing in the random polarization scenario. An upper bound of $\chi < 6.0 \times 10^{-16}$ is achieved at 26.96514 μeV, which is more than 3 orders of magnitude more stringent than the bound established by the QUALIPHIDE experiment. For a linear polarization scenario, the constraints depend on the angle between the polarization direction of the dark-photon field and the electric field [22]. Although the polarization of dark photons is unknown, the best and worst constraints can be obtained by going over all the possible polarization directions, as the blue, shallow green, and deep green regions in Fig. 4 show.

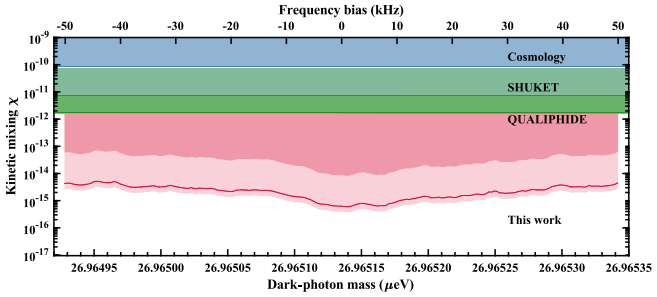

FIG. 4. Upper limits on the kinetic mixing between dark photons and ordinary photons. The red line refers to the upper bounds of the kinetic mixing in the random polarization scenario set by this work. The shallow and dark pink region refer to the excluded parameter space in the linear polarization scenario in the best and the worst condition, respectively. The tick marks at the top are the frequency biases from the central value, 6.52014 GHz, while the tick marks at the bottom are the corresponding dark-photon masses. The blue, shallow green, and deep green regions refer to the previous results of cosmological observations [38], the SHUKET [47] and the QUALIPHIDE [32] experiments, respectively. Data are adapted from [48].

In summary, we report an experimental search for dark photons, which is a possible candidate for dark matter. Our results improve the constraints of the kinetic mixing by more than 3 orders of magnitude. This work has shown an outstanding $\frac{Q_L Q_a}{Q_L+Q_a} VC \frac{\beta}{1+\beta}$ that is comparable with existing resonant haloscopes. For example, we have achieved an improvement of around 2 times compared with QUAX [26] and HAYSTAC [35]. However, this work is at a preliminary stage because of the lack of a tuning system. There is large room for improvement of $\frac{Q_L Q_a}{Q_L+Q_a} V^2 C^2 \frac{\beta^2}{(1+\beta)^2}$, which is more concerned with terms of scan rate. For future dark matter search experiments, new tunable cavities with larger mode volume are under construction. The sensitivity of our apparatus can be further improved by taking advantage of the single MW photon counting technique [49–51]. The searching efficiency can be multiplied by combining a series of cavities with different resonant frequencies. The experimental setup can also be used to test other predictions arising from new physics beyond the Standard Model, such as the existence of axions and axionlike particles, etc., with further upgrades [52,53]. In the future, it is practicable to examine the Kim-Shifman-Vainshtein-Zakharov model with the present setup, a superconducting cavity with through holes and 6 T magnet [54,55]. The sensitivity required by the Dine-Fischler-Srednicki-Zhitnitsky model is also within reach [56,57].

The authors are grateful to the anonymous referees for their valuable comments. This work was supported by the Innovation Program for Quantum Science and Technology (2021ZD0302200), the Chinese Academy of Sciences (No. GJJSTD20200001), the National Key R&D Program of China (Grants No. 2021YFB3202800, No. 2018YFA0306600, No. 2021YFC2203100), Anhui Initiative in Quantum Information Technologies (Grant No. AHY050000), NSFC (12150010, 12205290, 12261160569, 12261131497). Y. F. C. and M. J. thank the Fundamental Research Funds for Central Universities. Y. F. C. is supported in part by CAS Young Interdisciplinary Innovation Team (JCTD-2022-20), 111 Project (B23042). M. J. is supported in part by China Postdoctoral Science Foundation (2022TQ0330). This work was partially carried out at the USTC Center for Micro and Nanoscale Research and Fabrication.

[1] H. Poincare, The Milky Way and the theory of gases, Pop. Astron. **14**, 475 (1906).
[2] V. Trimble, Existence and nature of dark matter in the Universe, Annu. Rev. Astron. Astrophys. **25**, 425 (1987).
[3] J. L. Feng, Dark matter candidates from particle physics and methods of detection, Annu. Rev. Astron. Astrophys. **48**, 495 (2010).
[4] G. Bertone and D. Hooper, History of dark matter, Rev. Mod. Phys. **90**, 045002 (2018).
[5] A. Filippi and M. D. Napoli, Searching in the dark: The hunt for the dark photon, Rev. Phys. **5**, 100042 (2020).
[6] F. Zwicky, The redshift of extragalactic nebulae, Helv. Phys. Acta **6**, 110 (1933).
[7] A. Refregier, Weak gravitational lensing by large-scale structure, Annu. Rev. Astron. Astrophys. **41**, 645 (2003).
[8] M. Pospelov and J. Pradler, Big bang nucleosynthesis as a probe of new physics, Annu. Rev. Astron. Astrophys. **60**, 539 (2010).
[9] E. Komatsu *et al.*, Seven-Year Wilkinson Microwave Anisotropy Probe (WMAP) observations: Cosmological interpretation, Astrophys. J. Suppl. Ser. **192**, 18 (2011).
[10] J. Chang *et al.*, An excess of cosmic ray electrons at energies of 300–800 GeV, Nature (London) **456**, 362 (2008).
[11] I. Cholis, L. Goodenough, D. Hooper, M. Simet, and N. Weiner, High energy positrons from annihilating dark matter, Phys. Rev. D **80**, 123511 (2009).
[12] B. Abi *et al.*, Measurement of the positive muon anomalous magnetic moment to 0.46 ppm, Phys. Rev. Lett. **126**, 141801 (2021).
[13] C. Cazzaniga *et al.*, Probing the explanation of the muon $(g-2)$ anomaly and thermal light dark matter with the semi-visible dark photon channel, Eur. Phys. J. C **81**, 959 (2021).
[14] T. Aaltonen, High-precision measurement of the W boson mass with the CDF II detector, Science **376**, 170 (2022).
[15] A. W. Thomas and X. G. Wang, Constraints on the dark photon from parity violation and the W mass, Phys. Rev. D **106**, 056017 (2022).
[16] K.-Y. Zhang and W.-Z. Feng, Explaining the W boson mass anomaly and dark matter with a U(1) dark sector, Chin. Phys. C **47**, 023107 (2023).
[17] P. Galison and A. Manohar, Two Z's or not Two Z's?, Phys. Lett. **136B**, 279 (1984).
[18] B. Holdom, Two U(1)'s and ϵ charge shifts, Phys. Lett. **166B**, 196 (1986).
[19] B. Holdom, Searching for ϵ charges and a new U(1), Phys. Lett. B **178**, 65 (1986).
[20] P. Sikivie, Experimental tests of the "invisible" axion, Phys. Rev. Lett. **51**, 1415 (1983).
[21] P. Sikivie, Detection rates for "invisible"-axion searches, Phys. Rev. D **32**, 2988 (1985).
[22] A. Caputo, A. J. Millar, C. A. J. O'Hare, and E. Vitagliano, Dark photon limits: A handbook, Phys. Rev. D **104**, 095029 (2021).
[23] J. I. Read, The local dark matter density, J. Phys. G **41**, 063101 (2014).
[24] A. Quiskamp, B. T. McAllister, P. Altin, E. N. Ivanov, M. Goryachev, and M. E. Tobar, Exclusion of axionlike-particle cogenesis dark matter in a mass window above 100 μ eV, Phys. Rev. Lett. **132**, 031601 (2024).

[25] D. Alesini *et al.*, Search for invisible axion dark matter of mass $m_a = 43$ μeV with the QUAX–$a\gamma$ experiment, Phys. Rev. D **103**, 102004 (2021).
[26] D. Alesini *et al.*, Search for Galactic axions with a high-Q dielectric cavity, Phys. Rev. D **106**, 052007 (2022).
[27] R. Cervantes, G. Carosi, C. Hanretty, S. Kimes, B. H. LaRoque, G. Leum, P. Mohapatra, N. S. Oblath, R. Ottens, Y. Park, G. Rybka, J. Sinnis, and J. Yang, Search for 70 μeV dark photon dark matter with a dielectrically loaded multiwavelength microwave cavity, Phys. Rev. Lett. **129**, 201301 (2022).
[28] A. V. Dixit, S. Chakram, K. He, A. Agrawal, R. K. Naik, D. I. Schuster, and A. Chou, Searching for dark matter with a superconducting qubit, Phys. Rev. Lett. **126**, 141302 (2021).
[29] A. Andrianavalomahefa, C. M. Schafer, D. Veberic, R. Engel, T. Schwetz, H.-J. Mathes, K. Daumiller, M. Roth, D. Schmidt, R. Ulrich, B. Dobrich, J. Jaeckel, M. Kowalski, A. Lindner, and J. Redondo, Limits from the FUNK experiment on the mixing strength of hidden-photon dark matter in the visible and near-ultraviolet wavelength range, Phys. Rev. D **102**, 042001 (2020).
[30] J. Liu *et al.*, Broadband solenoidal haloscope for terahertz axion detection, Phys. Rev. Lett. **128**, 131801 (2022).
[31] S. Kotaka, S. Adachi, R. Fujinaka, S. Honda, H. Nakata, Y. Seino, Y. Sueno, T. Sumida, J. Suzuki, O. Tajima, and S. Takeichi, Search for dark photon dark matter in the mass range 74−110 μeV with a cryogenic millimeter-wave receiver, Phys. Rev. Lett. **130**, 071805 (2023).
[32] K. Ramanathan, N. Klimovich, R. B. Thakur, B. H. Eom, H. G. LeDuc, S. Shu, A. D. Beyer, and P. K. Day, Wideband direct detection constraints on hidden photon dark matter with the QUALIPHIDE experiment, Phys. Rev. Lett. **130**, 231001 (2023).
[33] F. Bajjali, S. Dornbusch, M. Ekmedzic, D. Horns, C. Kasemann, A. Lobanov, A. Mkrtchyan, L. H. Nguyen, M. Tluczykont, and G. Tuccari, First results from BRASS-p broadband searches for hidden photon dark matter, J. Cosmol. Astropart. Phys. 08 (2023) 077.
[34] A. Romanenko, R. Harnik, A. Grassellino, R. Pilipenko, Y. Pischalnikov, Z. Liu, O. S. Melnychuk, B. Giaccone, O. Pronitchev, T. Khabiboulline, D. Frolov, S. Posen, S. Belomestnykh, A. Berlin, and A. Hook, Search for dark photons with superconducting radio frequency cavities, Phys. Rev. Lett. **130**, 261801 (2023).
[35] B. M. Brubaker *et al.*, First results from a microwave cavity axion search at 24 μeV, Phys. Rev. Lett. **118**, 061302 (2017).
[36] D. Alesini *et al.*, Galactic axions search with a superconducting resonant cavity, Phys. Rev. D **99**, 101101(R) (2019).
[37] O. Kwon *et al.*, First results from an axion haloscope at CAPP around 10.7 eV, Phys. Rev. Lett. **126**, 191802 (2021).
[38] P. Arias, D. Cadamuro, M. Goodsell, J. Jaeckel, J. Redondo, and A. Ringwald, WISPy cold dark matter, J. Cosmol. Astropart. Phys. 06 (2012) 013.
[39] P. W. Graham, J. Mardon, and S. Rajendran, Vector dark matter from inflationary fluctuations, Phys. Rev. D **93**, 103520 (2016).
[40] P. A. R. Ade *et al.*, Planck2015 results, Astron. Astrophys. **594**, A20 (2016).
[41] Y. Tong, L. Wang, W. Zhang, M. Zhu, X. Qin, M. Jiang, X. Rong, and J. Du, A high performance fast-Fourier-transform spectrum analyzer for measuring spin noise spectrums, Chin. Phys. B **29**, 090704 (2020).
[42] See Supplemental Material at http://link.aps.org/supplemental/10.1103/PhysRevD.109.095037 for discussion of the experimental setup, calibration, and data analysis.
[43] S. Ghosh, E. P. Ruddy, M. J. Jewell, A. F. Leder, and R. H. Maruyama, Searching for dark photons with existing haloscope data, Phys. Rev. D **104**, 092016 (2021).
[44] C. M. Caves, Quantum limits on noise in linear amplifiers, Phys. Rev. D **26**, 1817 (1982).
[45] M. Kudra, J. Biznárová, A. F. Roudsari, J. J. Burnett, D. Niepce, S. Gasparinetti, B. Wickman, and P. Delsing, High quality three-dimensional aluminum microwave cavities, Appl. Phys. Lett. **117**, 070601 (2020).
[46] R. Cervantes, G. Carosi, S. Kimes, C. Hanretty, B. H. LaRoque, G. Leum, P. Mohapatra, N. S. Oblath, R. Ottens, Y. Park, G. Rybka, J. Sinnis, and J. Yang, ADMX-orpheus first search for 70 μeV dark photon dark matter: Detailed design, operations, and analysis, Phys. Rev. D **106**, 102002 (2022).
[47] P. Brun, L. Chevalier, and C. Flouzat, Direct searches for hidden-photon dark matter with the SHUKET experiment, Phys. Rev. Lett. **122**, 201801 (2019).
[48] C. A. J. O'Hare, AxionLimits, https://cajohare.github.io/AxionLimits/.
[49] K. Inomata, Z. Lin, K. Koshino, W. D. Oliver, J.-S. Tsai, T. Yamamoto, and Y. Nakamura, Single microwave-photon detector using an artificial Λ-type three-level system, Nat. Commun. **7**, 12303 (2016).
[50] B. Royer, A. L. Grimsmo, A. C.-Poitevin, and A. Blais, Itinerant microwave photon detector, Phys. Rev. Lett. **120**, 203602 (2018).
[51] L. Balembois, J. Travesedo, L. Pallegoix, A. May, and E. Billaud, Cyclically operated microwave single-photon counter with sensitivity of $10^{-22}\, W/\sqrt{Hz}$, Phys. Rev. Appl. **21**, 014043 (2024).
[52] L. D. Luzio, M. Giannotti, E. Nardi, and L. Visinelli, The landscape of QCD axion models, Phys. Rep. **870**, 1 (2020).
[53] P. Sikivie, Invisible axion search methods, Rev. Mod. Phys. **93**, 015004 (2021).
[54] J. E. Kim, Weak-interaction singlet and strong CP invariance, Phys. Rev. Lett. **43**, 103 (1979).
[55] M. A. Shifman, A. I. Vainshtein, and V. I. Zakharov, Can confinement ensure natural CP invariance of strong interactions?, Nucl. Phys. **B166**, 493 (1980).
[56] A. R. Zhitnitsky, Possible suppression of axion-hadron interactions, Sov. J. Nucl. Phys. **31**, 260 (1980).
[57] M. Dine, W. Fischler, and M. Srednicki, A simple solution to the strong CP problem with a harmless axion, Phys. Lett. **104B**, 199 (1981).